Int. J. Solids Structures Vol. 24, No. 7, pp. 705–722, 1988
Printed in Great Britain.

0020–7683/88 $3.00 + .00

AN ELASTOPLASTIC CONSTITUTIVE MODEL FOR CONCRETE

S. PIETRUSZCZAK, J. JIANG and F. A. MIRZA
Department of Civil Engineering and Engineering Mechanics, McMaster University, Hamilton, Ontario, Canada L8S 4L7

(*Received* 9 *January* 1987; *in revised form* 2 *February* 1988)

Abstract—A constitutive model for concrete, built within the framework of rate-independent theory of plasticity, is presented. The model invokes the concept of a failure locus which is introduced *a priori* as a path-independent criterion. The shape of the deviatoric section of this locus is influenced by the value of the confining pressure. The yield surface is assumed in a similar functional form to that of the failure locus, and its evolution is described in terms of a suitably chosen damage parameter. The plastic flow is governed by a non-associated flow rule. The material characteristics are strongly influenced by the actual confining pressure and display a smooth transition from a ductile to brittle behaviour. The procedure for identification of material parameters is explained in detail and the effectiveness of the concept is verified for a number of loading paths. The results of numerical simulations are compared with the experimental data available in the literature.

1. INTRODUCTION

A realistic solution to a structural problem involving plain or reinforced concrete depends, to a large extent, on the choice of an appropriate constitutive law. Consequently, in recent years considerable research has been focused on modelling of mechanical behaviour of concrete. The existing formulations have borrowed various theoretical frameworks from continuum mechanics: non-linear elasticity[1–3], rate-independent plasticity[4–6], endochronic theory[7, 8], as well as plastic-fracturing theory[9, 10].

The mechanical response of concrete is very complicated and it seems unlikely that any phenomenological approach will ever be able to embrace all possible variations in material characteristics. The objective of this paper is to propose a relatively simple rate-independent theory which adequately reflects certain typical trends in concrete behaviour. These include: a progressive transition from compaction to dilatancy, sensitivity of material characteristics to confining pressure including a continuous transition in failure mechanisms from ductile to brittle. The concept is built within the framework of the theory of elasto-plasticity. The deformation process is governed by a non-associated flow rule and involves a progressive evolution of the yield surface which is described in terms of an appropriate hardening/softening parameter.

In Section 2 basic assumptions incorporated in the formulation are outlined. The mathematical details concerning the form of failure, yield and plastic potential loci are provided, followed by a discussion of strain hardening/softening characteristics. The section is concluded by presenting the appropriate constitutive equations. Section 3 is concerned with identification of material parameters involved in the formulation. Finally, in Section 4, an extensive discussion on numerical effectiveness is provided. The performance of the model is verified for various loading histories imposed on different types of concrete.

2. A CONSTITUTIVE MODEL FOR CONCRETE

In order to provide a general mathematical formulation the following stress invariants are introduced:

$$I = -\sigma_{ii}; \quad \bar{\sigma} = (\tfrac{1}{2}s_{ij}s_{ij})^{1/2}$$

$$\theta = \tfrac{1}{3}\sin^{-1}\left(-\frac{3\sqrt{3}}{2}\frac{J_3}{\bar{\sigma}^3}\right); \quad -\pi/6 \leqslant \theta \leqslant \pi/6. \tag{1}$$

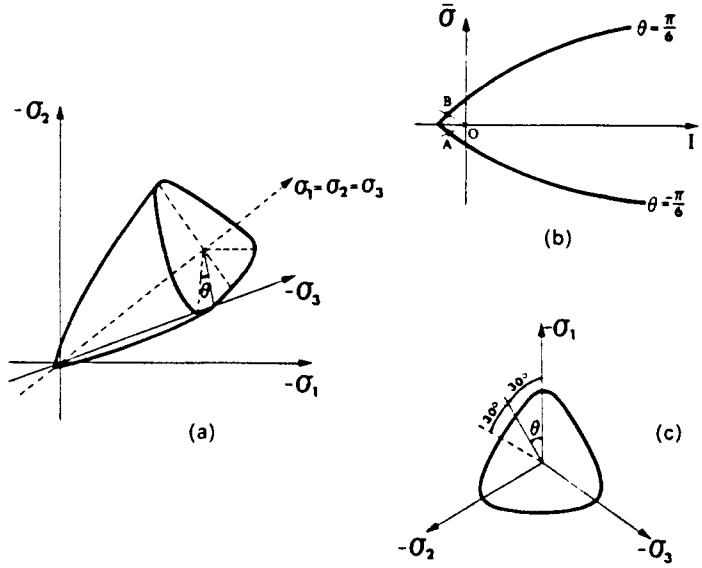

Fig. 1. Failure surface in (a) principal stress space; (b) meridional plane; (c) deviatoric plane (π-plane).

In the equations above $s_{ij} = \sigma_{ij} - 1/3\delta_{ij}\sigma_{kk}$ denotes the stress deviator, whereas θ represents the angle measure of the third stress invariant $J_3 = 1/3 s_{ij}s_{jk}s_{ki}$.

The proposed description invokes the concept of a path-independent failure (limit) locus, $F(\sigma_{ij}) = 0$ which is introduced *a priori*. The progressive deformation of the material is described in terms of evolution of the family of yield surfaces, $f(\sigma_{ij}, \xi) = 0$, where ξ is a suitably defined damage parameter. The instantaneous direction of plastic flow is determined by a non-associated flow rule, which involves the existence of the family of plastic potential surfaces defined in a parametric form $\Psi(\sigma_{ij}) = \text{const}$. The material characteristics are largely affected by the value of the confining pressure. The formulation assumes a smooth transition from a ductile (stable) to a brittle (unstable) response. This is enforced by selecting an appropriate form of strain hardening/softening function. In what follows, major assumptions embodied in the proposed concept are outlined together with relevant mathematical details.

2.1. *Failure (or limit) locus*

Failure criterion defines maximum strength of concrete under any possible combination of stresses. It is assumed that this criterion is not influenced by the deformation history and can be postulated *a priori*. Based on existing experimental evidence[11], the following form of the failure locus is proposed:

$$F = a_1\left(\frac{\bar{\sigma}}{g(\theta)f_c}\right) + a_2\left(\frac{\bar{\sigma}}{g(\theta)f_c}\right)^2 - \left(a_3 + \frac{I}{f_c}\right) = 0 \tag{2}$$

where a_1, a_2, and a_3 are dimensionless material constants, whereas f_c represents uniaxial compressive strength of concrete.

In the principal stress space eqn (2) represents an irregular cone with smooth curved meridians and a non-circular convex cross-section in the deviatoric (π) plane (Fig. 1). The shape of the π-plane sections (defined through the function $g(\theta)$) is assumed to be strongly influenced by the value of the confining pressure. The function $g(\theta)$ is selected in the form proposed in Ref. [12]

$$g(\theta) = \frac{(\sqrt{(1+a)} - \sqrt{(1-a)})K}{K\sqrt{(1+a)} - \sqrt{(1-a)} + (1-K)\sqrt{(1-a\sin 3\theta)}}; \quad a = \text{const.} \quad (a \to 1) \tag{3}$$

which satisfies $g(\pi/6) = 1$ and $g(-\pi/6) = K$ and for $a = 0.999$ guarantees convexity for

$K \geqslant 0.565$ (see Ref. [12]). Other suitable representations of $g(\theta)$ are discussed in Refs [12, 13]. In eqn (3) $K = \bar{\sigma}_t/\bar{\sigma}_c$, where $\bar{\sigma}_c$ and $\bar{\sigma}_t$ represent the maximum values of $\bar{\sigma}$, for $I = \text{const.}$, in compression ($\theta = \pi/6$) and extension ($\theta = -\pi/6$) domains, respectively. In the present study $K = K(I)$ is assumed and the following simple function describing variation of K is chosen

$$K = 1 - K_0 \, e^{-K_1(a_3 + I/f_c)} \tag{4}$$

where K_0 and K_1 are material constants. It should be noted that according to eqns (3) and (4) the shape of the π-plane section changes from a curvilinear triangle for low hydrostatic pressures to nearly circular at high pressures ($I \to \infty$ implies $K \to 1$ in eqn (4)).

For a further discussion it is convenient to write eqn (2) in the following parametric form:

$$F = \bar{\sigma} - g(\theta)\bar{\sigma}_c = 0 \tag{5}$$

where

$$\bar{\sigma}_c = \frac{-a_1 + \sqrt{(a_1^2 + 4a_2(a_3 + I/f_c))}}{2a_2} f_c.$$

2.2. *Yield loci*

In order to define the family of yield loci a similar functional form as that in eqn (5) is employed, i.e.

$$f = \bar{\sigma} - \beta(\xi) g(\theta)\bar{\sigma}_c = 0 \tag{6}$$

where $\beta(\xi)$ represents a hardening/softening function and ξ is a suitably chosen damage parameter. In a ductile regime (at relatively high confining pressures), in which material characteristics are stable, the function $\beta(\xi)$ is selected in the hyperbolic form

$$\beta(\xi) = \frac{\xi}{A + B\xi} \tag{7}$$

where A and B represent material constants and ξ is defined by

$$d\xi = \frac{d\bar{\varepsilon}^p}{\Phi}; \quad \xi = \int d\xi. \tag{8}$$

In eqn $(8)_1$, $d\bar{\varepsilon}^p$ is a measure of plastic distortions

$$d\bar{\varepsilon}^p = (de_{ij}^p \, de_{ij}^p)^{1/2}; \quad de_{ij}^p = d\varepsilon_{ij}^p - \tfrac{1}{3}\delta_{ij} \, d\varepsilon_{kk}^p$$

whereas $\Phi = \text{const.}$ is a factor defined through a parametric equation

$$\Phi(I, \theta) = \left[g(\theta)\left(a_3 + \frac{I}{f_c}\right)\right]^2 = \Phi. \tag{9}$$

Incorporation of Φ in eqn (8) is motivated by the experimental evidence. The proposed functional form eqn (9), allows typical trends in the variation of material characteristics with both I and θ to be simulated, as discussed later in this paper.

It should be noted that, according to eqn (7), $\beta(\xi) \to 1$ as $\xi \to \infty$ (since $B \approx 1$, eqn $(30)_2$ in the next section), which implies that the yield surface asymptotically approaches

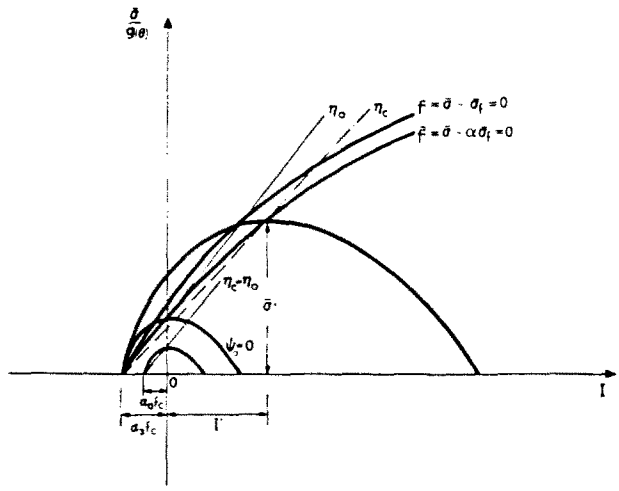

Fig. 2. Plastic potential surface in meridional plane.

the failure surface. On the other hand, $\beta(\xi) = 0$ for $\xi = 0$, which indicates that, in the proposed approach, the size of the initial yield surface is reduced to zero.

2.3. *Plastic potential surface*

Experimental evidence suggests that in a ductile regime a smooth transition from compaction to dilatancy takes place prior to failure. A similar trend is also observed in certain geological materials (e.g. dense sand) and can be adequately modelled by assuming a non-associated flow rule and defining an appropriate form of the plastic potential[14]. Recognizing this analogy, the plastic potential function is adopted in a similar form to that proposed in Ref. [14], i.e.

$$\Psi = \bar{\sigma} + \eta_c g(\theta)\bar{I} \ln\left(\frac{\bar{I}}{\bar{I}_0}\right) = 0 \tag{10}$$

where $\bar{I} = a_0 f_c + I$ and a_0 is a constant which defines the location of the apex of the plastic potential surface in the tensile domain. Moreover, the parameter η_c represents the value of $\eta = \bar{\sigma}/(g(\theta)\bar{I})$ at which the transition from compaction to dilatancy occurs (at $\eta = \eta_c$, $d\varepsilon_v^p = 0$). It is assumed that such transition takes place along the locus

$$\bar{f} = \bar{\sigma} - \chi g(\theta)\bar{\sigma}_c = 0 \tag{11}$$

in which χ is a material constant.

Figure 2 shows the meridional section of the family of plastic potential surfaces. In order to satisfy the condition of irreversibility following from the second law of thermodynamics, i.e. $\sigma_{ij}\, d\varepsilon_{ij}^p \geqslant 0$, all surfaces must be convex with respect to the origin of the stress space. To comply with the latter requirement an appropriate evolution law for the set of $\Psi = 0$ defined by eqn (10) must be provided. Denote by η_0 the value of η_c at $I = 0$ and $a_0 = a_3$

$$\eta_0 = \frac{\chi(-a_1 + \sqrt{(a_1^2 + 4a_2 a_3)})}{2a_2 a_3} \tag{12}$$

and let the corresponding plastic potential surface, eqn (10), be $\Psi_0 = 0$ (Fig. 2). It is assumed that for $\eta_c < \eta_0$ all subsequent plastic potential surfaces are obtained by an isotropic expansion of $\Psi_0 = 0$ under $a_0 = a_3 = \text{const}$. If the stress point falls inside the domain enclosed by $\Psi_0 = 0$ the family of $\Psi = 0$ satisfies the constraints $\eta_c = \eta_0$, $a_0 < a_3$. The latter assumption implies that inside $\Psi_0 = 0$ all subsequent loci are reduced in size

and the apex gradually migrates towards the origin, $0 \leqslant a_0 \leqslant a_3$. Mathematical details concerned with identification of the current plastic potential are provided in Appendix A.

2.4. *Strain softening response*

The mechanical response of concrete is largely influenced by the value of confining pressure. At relatively high pressures, a pattern of numerous microcracks develops and material characteristics display a stable nature. As the confining pressure decreases, a gradual transition from ductile to brittle behaviour takes place. In the brittle regime, distinct macrocracks form, generating an unstable material response.

In the present concept the transition from a stable (ductile) to unstable (brittle) response is modelled by an appropriate generalization of the hardening function (eqn (7)). The form of this function is suitably selected to reflect a gradual change in material characteristics from strain hardening (for high confining pressures) to strain softening with progressively increasing rate.

Assume the following generalization of the function $\beta(\xi)$ specified by eqn (7):

$$\beta(\xi) = \frac{\xi}{A + B\xi}[1 - \bar{\phi}_r(1 - e^{-C\langle \xi - \xi_f \rangle^\gamma})] \tag{13a}$$

where

$$C = \bar{\phi}_r H\left[\left\langle \frac{(I/f_c)_\Gamma - (I/f_c)_f}{a_3 + (I/f_c)_f} \right\rangle\right]^\mu \tag{13b}$$

and angular brackets $\langle\ \rangle$ are defined according to

$$\langle x \rangle = \begin{cases} 0 & \text{if } x \leqslant 0 \\ x & \text{if } x > 0. \end{cases} \tag{14}$$

In eqns (13) ξ_f represents the value of ξ corresponding to the maximum value of $\beta = \beta_f$, $(I/f_c)_f$ is evaluated at $\beta = \beta_f$ and $(I/f_c)_\Gamma$ denotes a normalized value of confining pressure at which a transition from ductile to brittle behaviour takes place. Moreover, γ, μ and H represent material constants and $\bar{\phi}_r$ defines the residual strength of the material.

According to eqn (13a), the inception of strain softening takes place at $\xi = \xi_f$. In this paper, the transition to unstable behaviour has been described in terms of a path-independent criterion $F \to 0$ under $I < I_\Gamma$. In general, however, the value of ξ_f can be determined more rigorously using an appropriate strain localization criterion derived from considerations of stability of the constitutive relation (bifurcation problem, see e.g. Ref. [15]). The latter approach is currently under investigation.

The constant C, specified by eqn (13b), controls the rate of strain softening in the post-bifurcation mode. After inception of strain localization, the sample is no longer homogeneous and to model precisely its response one should refer to a boundary value problem. The approach advocated here is based on the concept of an equivalent continuum, similar to that introduced in Ref. [16]. Strain softening is viewed as a local phenomenon occurring in a "smeared" sense at a material point. Equation (13b) incorporates the "size effect" by employing constant $\bar{\phi}_r$ which associates the rate of softening with the relative volume of the sample, selected here as a characteristic dimension. Specification of $\bar{\phi}_r$ is discussed in detail in Appendix B.

It can be shown that, according to eqns (13), for $\gamma > 1.0$, the following conditions are satisfied:

$$\left.\frac{d\beta}{d\xi}\right|_{\xi=\xi_f^+} = \left.\frac{d\beta}{d\xi}\right|_{\xi=\xi_f} ; \quad \lim_{\xi\to\infty}\beta \approx 1-\bar{\phi}_r. \tag{15}$$

It is also evident that for $C = 0$ ($I \geqslant I_T$) eqns (13) reduce to eqn (7) (strain hardening response), whereas $I \to -a_3 f_c$ implies $C \to \infty$ which leads to a perfectly brittle response. Hence, the function defined in eqns (13) satisfies all mathematical requirements for a continuous change of material characteristics from ductile to brittle.

In the strain softening range, the deformation process is again described in terms of a non-associated flow rule with the plastic potential specified by eqn (10). The zero dilatancy locus, as defined in the stable regime by eqn (11), is assumed to undergo gradual contraction with a decreasing value of β

$$\bar{f} = \bar{\sigma} - \beta\chi g(\theta)\bar{\sigma}_c = 0. \tag{16}$$

The above functional form enables the modelling of progressive dilation of the material during the unstable phase.

Finally, in the brittle regime, the non-uniform deformation mode consists of either sliding along asperities or, in certain circumstances, an abrupt fracture, i.e. opening of a tensile microcrack. The former mechanism is completely described by eqns (13) and (15), whereas the latter one involves an instantaneous reduction of all stress components to zero. The fracture domain (OAB) is shown schematically in Fig. 1(b). If the stress path, after reaching the failure surface, penetrates into this domain, an abrupt fracture takes place. If, on the other hand, the residual strength envelope (as implicitly defined by $\bar{\phi}_r$) is reached first, an unlimited plastic flow commences. At this time, the extent of the fracture domain cannot be precisely defined due to lack of adequate experimental data. One can speculate only that this domain is confined to a vicinity of the tensile branch of the hydrostatic axis.

2.5. *Formulation of constitutive equations*

Assuming additivity postulate between the elastic and plastic strain increments, a generalized Hook's law can be written as

$$d\sigma_{ij} = D^e_{ijkl}(d\varepsilon_{kl} - d\varepsilon^p_{kl}) \tag{17}$$

where D^e_{ijkl} represents the elastic constitutive matrix. During an active loading process, the consistency condition $df = 0$ has to be satisfied, i.e.

$$\frac{\partial f}{\partial \sigma_{ij}} d\sigma_{ij} + \frac{\partial f}{\partial \beta}\frac{d\beta}{d\xi} d\xi = 0 \tag{18}$$

in which $f(\sigma_{ij}, \xi) = 0$ is defined according to eqn (6). Introducing the non-associated flow rule

$$d\varepsilon^p_{ij} = d\lambda \frac{\partial \Psi}{\partial \sigma_{ij}} \tag{19}$$

the differential $d\xi$, defined by eqn $(8)_1$, can be written in the following form:

$$d\xi = d\lambda \left(\operatorname{dev}\frac{\partial \Psi}{\partial \sigma_{ij}} \operatorname{dev}\frac{\partial \Psi}{\partial \sigma_{ij}} \right)^{1/2} \Big/ \Phi \tag{20}$$

in which dev $\partial\Psi/\partial\sigma_{ij}$ represents the deviatoric part of $\partial\Psi/\partial\sigma_{ij}$, with $\Psi(\sigma_{ij}) = \text{const.}$ given by eqn (10). Thus, substituting eqn (17) into eqn (18) and utilizing eqn (20) one obtains

$$d\lambda = \frac{1}{H_e + H_p}\left(\frac{\partial f}{\partial \sigma_{ij}} D^e_{ijkl}\, d\varepsilon_{kl}\right) \tag{21}$$

where

$$H_p = -\frac{\partial f}{\partial \beta}\frac{d\beta}{d\xi}\frac{\left(\operatorname{dev}\dfrac{\partial \Psi}{\partial \sigma_{ij}} \operatorname{dev}\dfrac{\partial \Psi}{\partial \sigma_{ij}}\right)^{1/2}}{\Phi}; \quad H_e = \frac{\partial f}{\partial \sigma_{pq}} D^e_{pqrs}\frac{\partial \Psi}{\partial \sigma_{rs}} \tag{22}$$

and H_p represents the plastic hardening/softening modulus. The mathematical details concerned with the determination of H_p are provided in Appendix A.

The parameter $d\lambda$ can also be defined in terms of stress increment $d\sigma_{ij}$. Introducing eqn (20) directly into eqn (18) yields

$$d\lambda = \frac{1}{H_p}\left(\frac{\partial f}{\partial \sigma_{ij}} d\sigma_{ij}\right). \tag{23}$$

Finally, substitution of eqn (21) in eqn (17) leads to the constitutive equation in a conventional form

$$d\sigma_{ij} = \left(D^e_{ijkl} - \frac{D^e_{ijpq}\dfrac{\partial \Psi}{\partial \sigma_{pq}}\dfrac{\partial f}{\partial \sigma_{mn}} D^e_{mnkl}}{H_e + H_p}\right) d\varepsilon_{kl}. \tag{24}$$

Equation (24) describes an active loading process during which irreversible deformations are generated. In the hardening regime, $H_p > 0$, such loading histories are constrained to stress paths satisfying

$$f = 0 \quad \text{and} \quad \frac{\partial f}{\partial \sigma_{ij}} d\sigma_{ij} > 0. \tag{25}$$

It should be noted that inequality (25) implies $d\lambda > 0$ in eqn (23). This ensures (in view of convexity of the plastic potential, eqn (10)), that the energy dissipated during plastic flow is always positive.

In the softening regime $H_p < 0$, the postulate of irreversibility again requires positiveness of $d\lambda$. In order to distinguish between loading and elastic unloading, definition (21) can be implemented, yielding

$$f = 0 \quad \text{and} \quad \frac{\partial f}{\partial \sigma_{ij}} D^e_{ijkl}\, d\varepsilon_{kl} > 0 \tag{26}$$

as the criterion for an active process. According to this inequality plastic deformations will occur whenever the stress increment obtained from the elastic solution $d\sigma'_{ij} = D_{ijkl}\, d\varepsilon_{kl}$, is directed outside of the yield surface. Criterion (26) is restricted to cases when $H_e + H_p > 0$, i.e. there exists a locally unique response in stress rate for any specified strain rate. It should be noted that for $H_e + H_p \leqslant 0$, the deformation process ceases to be locally controllable. The question of static admissibility of the present formulation is addressed further in Appendix B.

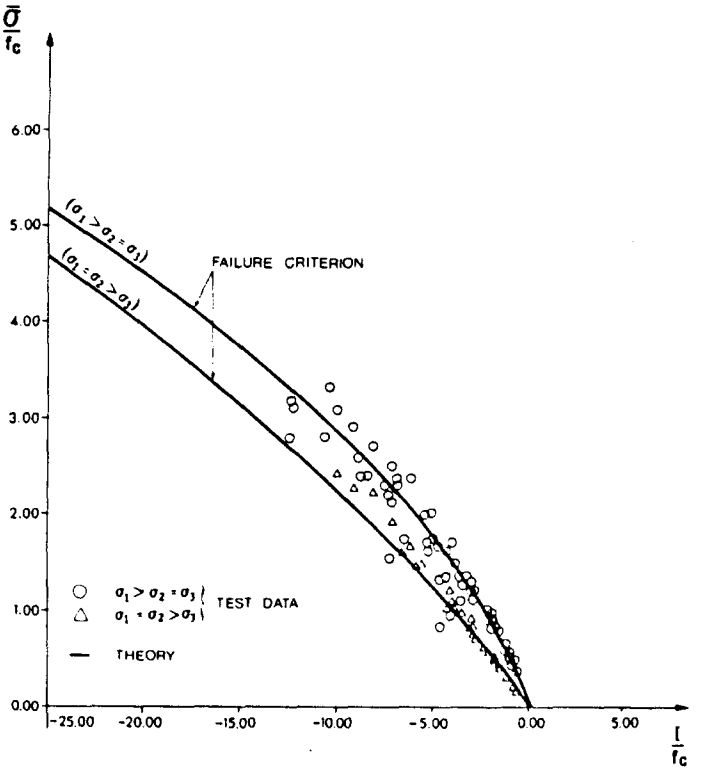

Fig. 3. Meridional sections of the failure locus (for $\theta = \pm\pi/6$).

3. IDENTIFICATION OF MATERIAL PARAMETERS

The proposed constitutive model involves the following material parameters:

(a) parameters a_1, a_2, a_3, K_0 and K_1, defining the failure envelope (eqn (2));

(b) parameters A and B, involved in the strain hardening function (eqn (7));

(c) parameters H, γ, μ, associated with the strain softening response, as well as transition pressure $(I/f_c)_t$, and parameters $\bar{\phi}_r$, $\bar{\phi}$, (eqns (13));

(d) dilatancy parameter α (eqn (11)).

In addition, the elastic properties should also be specified, namely Young's modulus, E, and Poisson's ratio, ν.

Most of the above listed parameters can be determined *a priori* based on extensive experimental data available in the literature. Thus, the effective number of parameters required to identify the model can be significantly reduced. The details concerning the identification procedure (based on the experimental data from Refs [3, 17–22]) are summarized below.

3.1. *Parameters defining the failure envelope*

The constants a_1, a_2, a_3, K_0 and K_1 are related to the form of the failure locus. In order to identify these parameters two steps were followed. First, along the compressive meridian ($\theta = \pi/6$), eqn (2) was fitted to the data provided in Refs [3, 19–22] by the least square approach. It was assumed that $a_3 = 0.3$, which corresponds to $f_t = 0.1f_c$, with f_t representing the uniaxial tensile strength of concrete. Subsequently, the form of the extension branch ($\theta = -\pi/6$) was determined. In this case, two failure states were chosen to be satisfied exactly, namely: uniaxial tension $f_t = 0.1f_c$ and a biaxial compression $f_{bc} = -1.16f_c$[18]. Thus, throughout the identification process, f_c (i.e. uniaxial compressive strength) was assumed as the only independent parameter.

The procedure described above resulted in the following values of the constants:

$$a_1 = 1.9253, \quad a_2 = 0.5635, \quad a_3 = 0.3, \quad K_0 = 0.43416, \quad K_1 = 0.07439. \tag{27}$$

Figure 3 presents meridional sections of the failure locus in both compressions and extension domains. The plot is normalized with respect to f_c and the proposed analytical form is compared with the experimental data provided in Refs [3, 19–22].

When selecting the material constants according to eqns (27), the only information required to identify the form of the failure locus is that concerning the value of f_c. In the case when the results of a uniaxial tension test are also available, an exact value of f_t can be used instead of an average approximation $f_t = 0.1 f_c$. Substituting the conditions of uniaxial tension ($\sigma_1 = f_t$, $\sigma_2 = \sigma_3 = 0$) and biaxial compression ($\sigma_1 = \sigma_2 = f_{bc}$, $\sigma_3 = 0$) in eqns (4) and (5) leads to the following modifications of parameters a_3, K_0 and K_1 (eqns (2) and (4)):

$$\begin{aligned} a_3 &= 3\frac{f_t}{f_c} \\ K_1 &= \frac{1}{(f_t/f_c) - 2(f_{bc}/f_c)} \ln\left(\frac{1-K_t}{1-K_{bc}}\right) \\ K_0 &= (1-K_t)\, e^{2K_1(f_t/f_c)} \end{aligned} \tag{28}$$

where K_t and K_{bc} represent the values of K corresponding to uniaxial tension and biaxial compression, respectively

$$\begin{aligned} K_t &= \frac{2\sqrt{3}}{3} \frac{a_2 f_t/f_c}{-a_1 + \sqrt{(a_1^2 + 8a_2 f_t/f_c)}} \\ K_{bc} &= -\frac{2\sqrt{3}}{3} \frac{a_2 f_{bc}/f_c}{-a_1 + \sqrt{(a_1^2 + 4a_2(3f_t/f_c - 2f_{bc}/f_c))}} \end{aligned} \tag{29}$$

and $f_{bc} = -1.16 f_c$, according to Ref. [18].

3.2. *Hardening function parameters*

The expression defining the hardening function, eqn (7), contains two material constants A and B. Both parameters can be identified by fitting eqn (7) to the test data plotted in the $(\bar{\sigma}/\bar{\sigma}_t, \bar{\varepsilon}^p)$ plane, where $\bar{\sigma}_t = g(0)\bar{\sigma}_c$. Using the data from a series of I = const. tests provided in Ref. [17], the following values were arrived at:

$$A = 0.000085; \quad B = 0.95. \tag{30}$$

The results of the numerical simulations showing the variations of $\beta - \bar{\varepsilon}^p$ characteristics in both compression and extension programs, are presented in Figs 4(a) and (b), respectively.

In the subsequent section, predictions of numerous experimental tests for different types of concrete (f_c ranging from 15.3 to 62.1 N mm^{-2}) are provided. The results allow one to speculate that the values of A and B as defined by eqns (30) are not affected by the actual uniaxial strength of the material and can be adopted *a priori*.

3.3. *Dilatancy parameter*

This parameter defines the locus along which the transition from compaction to dilatancy takes place (eqn (11)). Experimental evidence indicates (e.g. Refs [17, 18]) that in various types of concrete the maximum volumetric strain is reached at approximately 95% of the failure stress. Consequently, $\alpha = 0.95$ may be assumed in eqn (11).

3.4. *Strain softening parameters*

At the present time, the parameters, H, μ, γ and $(I/f_c)_T$, eqns (13a) and (13b), cannot be determined precisely due to lack of adequate experimental data. The existing experimental evidence[3, 23], however, supports the proposed conceptual framework, i.e.

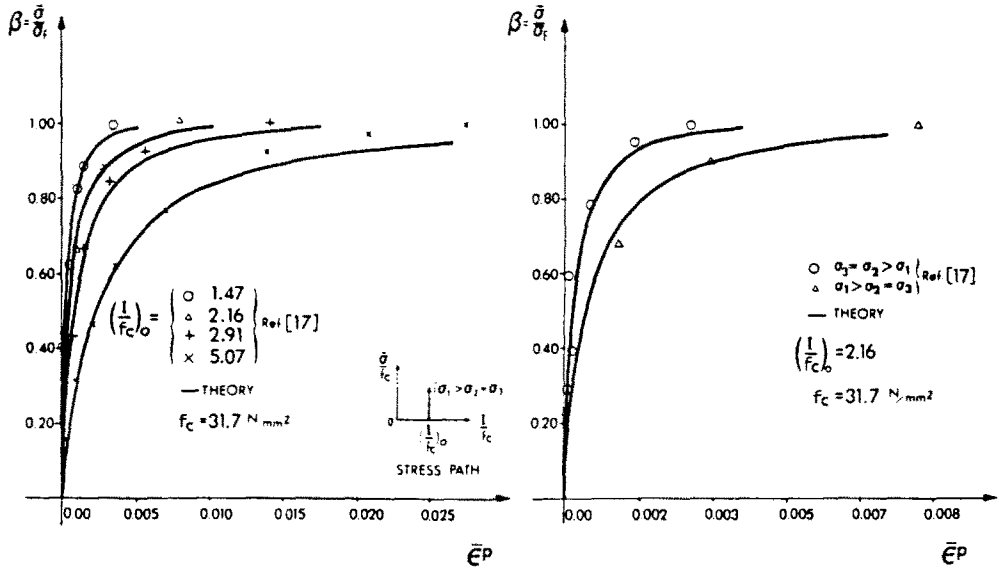

Fig. 4. Numerical simulations of a series of I = const. tests[17].

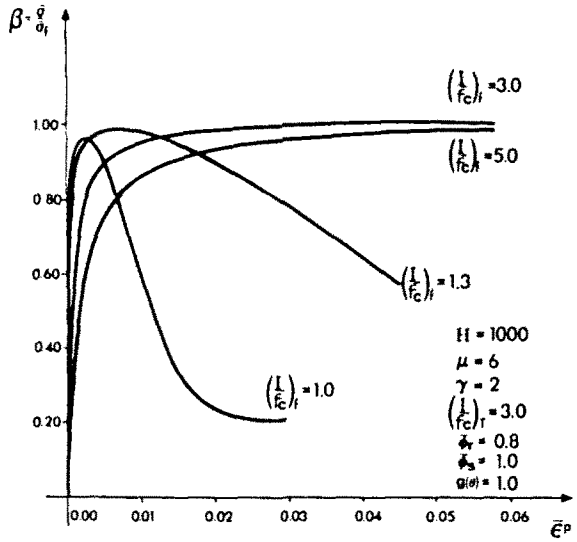

Fig. 5. Predicted variations in material characteristics with confining pressure.

there is a brittle-ductile transition value of confining pressure $(I/f_c)_T$, which corresponds to initiation of the strain softening response.

Assume $\gamma = 2$, which satisfies requirements imposed by eqn (15). Then, the rate of strain softening is controlled by H and μ. Both these constants can be determined from, e.g. a uniaxial compression test by matching (trial and error process) the actual strain softening characteristic. The parameter $\bar{\phi}_r$, eqns (13a) and (15), defines implicitly the form of the residual strength envelope. It is recognized that $\bar{\phi}_r$ may depend on the confining pressure through a parametric equation $\bar{\phi}_r = \phi_r(I) = \text{const}$. It seems however, that a sufficient accuracy in numerical predictions may be attained by assuming $\bar{\phi}_r = \text{const.}$, which implies that the residual strength locus has a similar analytical form to that of the yield surface. Experimental investigations reported in Refs [24, 25] indicate that

$$\lim_{\bar{\varepsilon}^p \to \infty} \beta = 0.2 \sim 0.3$$

for both uniaxial tension and uniaxial compression tests. Consequently, according to eqn (15), $\bar{\phi}_r = 0.7 \sim 0.8$ may be assumed in eqn (13a).

Figure 5 shows the variation of material characteristics with the confining pressure as

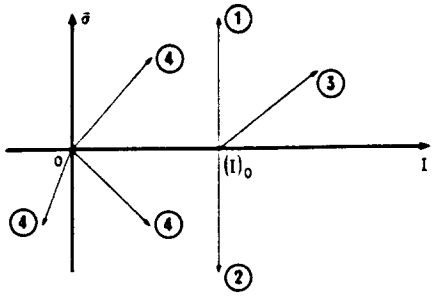

Fig. 6. Various loading paths considered in numerical simulations.

predicted by the proposed model. For the strain softening branch, some arbitrary values of $H = 1000$ and $\mu = 6$ ($\beta_f = 0.95$) were selected in order to demonstrate the basic trends in material response. The simulations were completed assuming $\bar{\phi}_s = 1$ in eqn (13b). The influence of this parameter is discussed in detail in Appendix B. The obtained characteristics are, in a qualitative sense, quite satisfactory and reflect a smooth ductile–brittle transition.

4. NUMERICAL PREDICTIONS

In this section the effectiveness of the proposed model is verified for a number of loading paths imposed on different types of concrete (f_c ranging from 15.3 to 62.1 N mm^{-2}). The loading histories considered are indicated in Fig. 6 and include:

Path 1: hydrostatic compression followed by loading along the compressive meridian under $d\bar{\sigma} > 0, I = \text{const}$.

Path 2: hydrostatic compression followed by loading into the extension domain under $d\bar{\sigma} > 0, I = \text{const}$.

Path 3: hydrostatic compression followed by uniaxial compression (under $\sigma_2 = \sigma_3 = \text{const}$.).

Path 4: proportional loading histories: uniaxial tension, uniaxial compression, biaxial tension and biaxial compression.

The results of numerical simulations are presented in Figs 7–12. The predictions in Figs 7–11 are restricted to the strain-hardening regime (due to lack of sufficient experimental data). Figures 7 and 8 show simulations for stress paths 1 and 2, respectively. Some of these

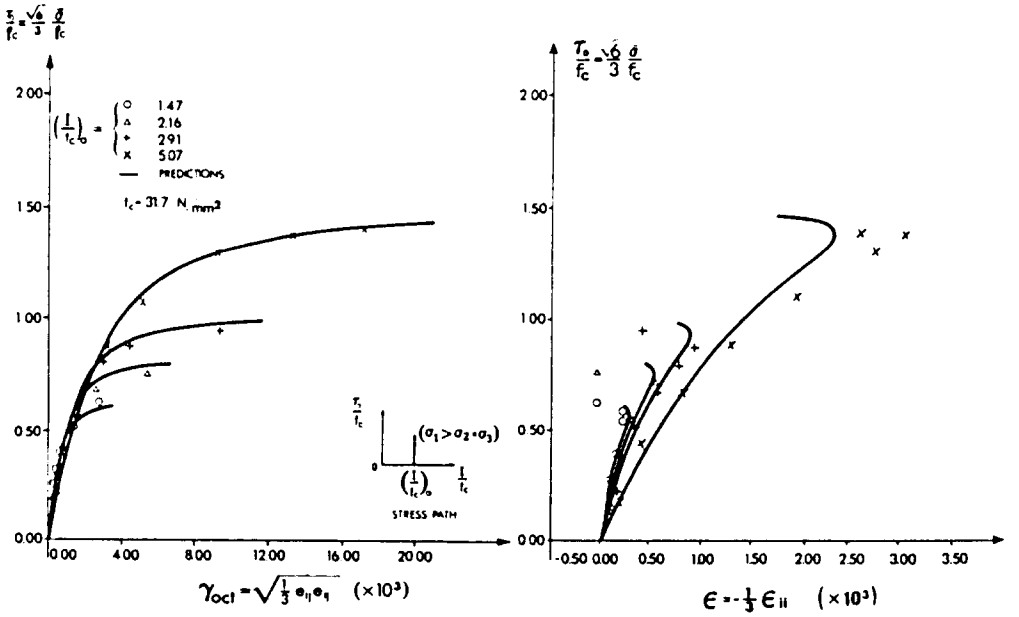

Fig. 7. Numerical simulations of various compression programs under $I = \text{const}$.[17].

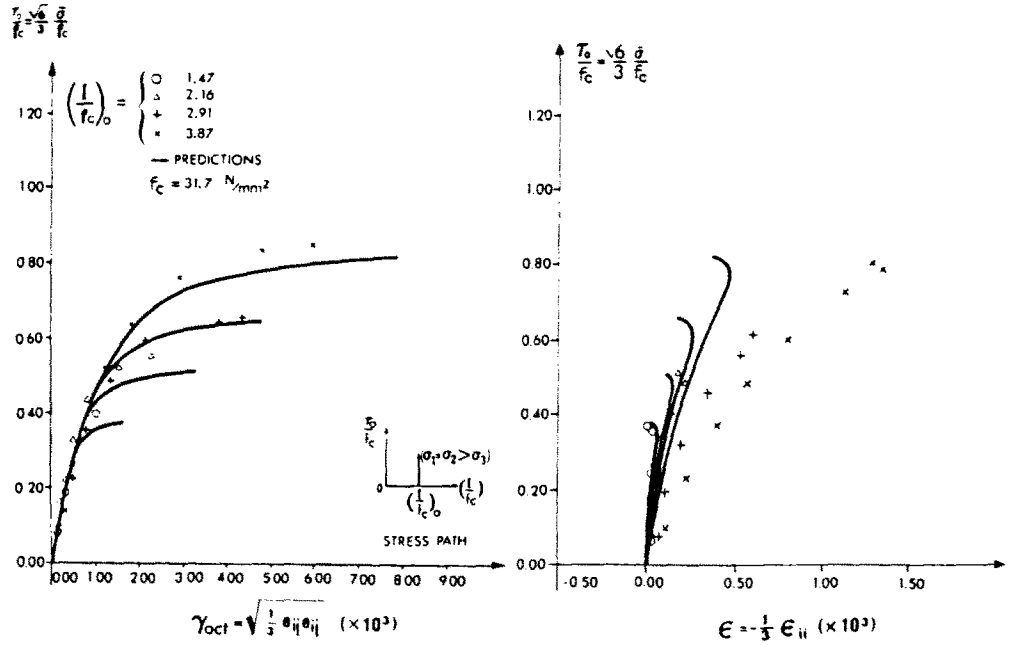

Fig. 8. Numerical simulations of a series of extension programs under I = const.[17].

results have already been referred to in Section 3 for the purpose of identification of material parameters. Figures 7(a) and 8(a) show the normalized deviatoric characteristics, whereas Figs 7(b) and 8(b) present the corresponding volume change. Numerical predictions are compared with the experimental data provided in Ref. [17]. Figure 9 presents the predictions corresponding to path 3. The behaviour of two different types of concrete is simulated (f_c = 15.3 and 62.1 N mm $^{-2}$) under different confining pressures. A complete stress–strain history is provided and the results are compared with those quoted in Ref. [17]. Subsequently Figs 10 and 11 are concerned with uniaxial and biaxial programs at zero confining pressures (paths 4). Figure 10 shows the material characteristics as predicted in compression tests, whereas Fig. 11 refers to extension programs. Experimental data from Ref. [18] are used for comparison. Finally, Fig. 12 presents the simulation of another uniaxial compression test (at I = 0 initially) as performed by Wang *et al.*[26]. In this case, a complete deformation history is traced including the unstable branch. Prior to failure, the material undergoes

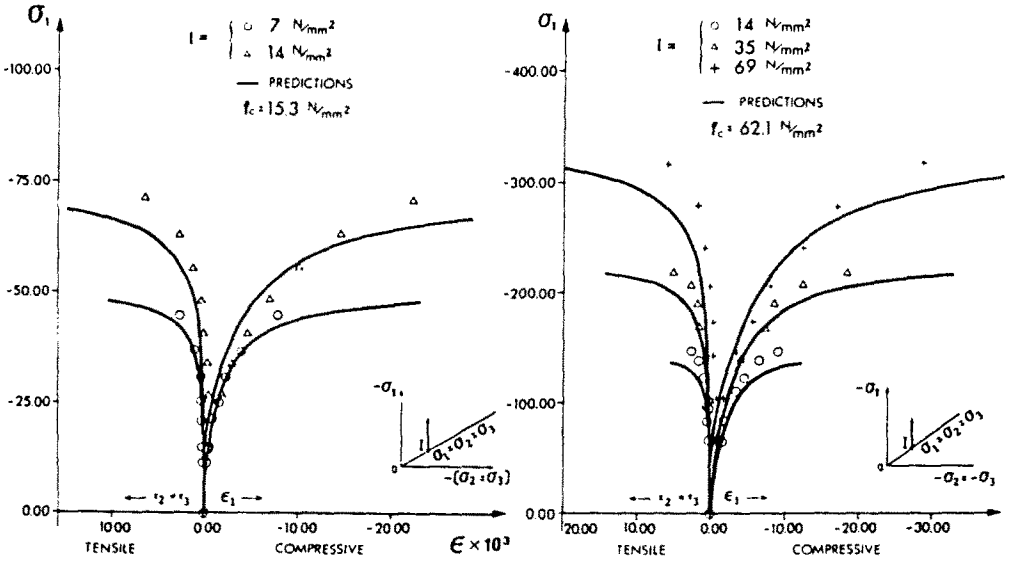

Fig. 9. Predictions for various uniaxial compression tests at different confining pressures[17]: (a) f_c = 15.3 N mm^{-2}; (b) f_c = 62.1 N mm^{-2}

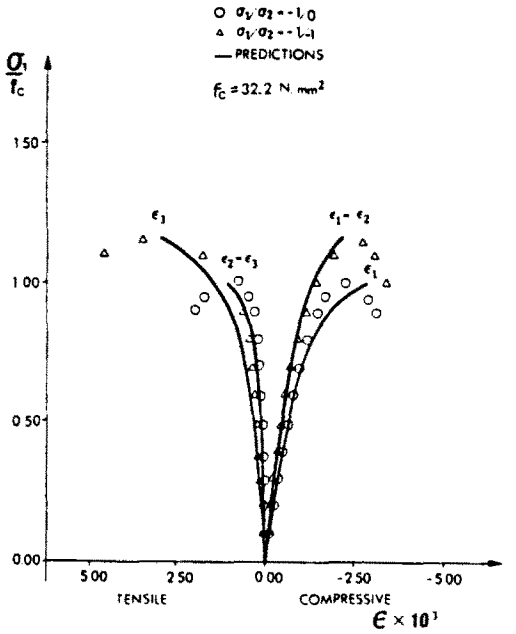

Fig. 10. Numerical simulations of uniaxial and biaxial compression tests[18].

compaction with progressively decreasing rate. During the strain softening phase, a significant dilation is predicted which is in accordance with the existing experimental evidence[27].

In general, for the cases presented, the agreement between the numerical simulations and the experimental data is quite satisfactory. For high confining pressures the model tends to underpredict the volumetric strains (Fig. 8(b)). To improve the performance in that respect the form of plastic potential would have to be altered accordingly. The observed discrepancy is not very significant however, to justify further complications in the formulation.

5. CONCLUSIONS

A relatively simple rate-independent plasticity model has been presented for predicting the behaviour of concrete under a general three-dimensional stress state. The model captures

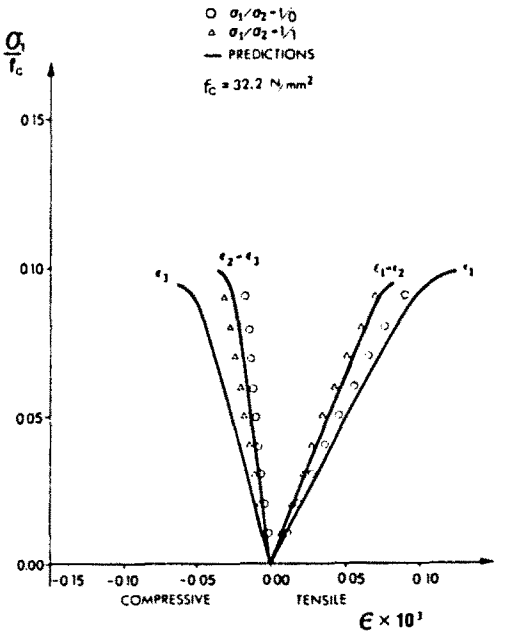

Fig. 11. Numerical simulations of uniaxial and biaxial extension tests[18].

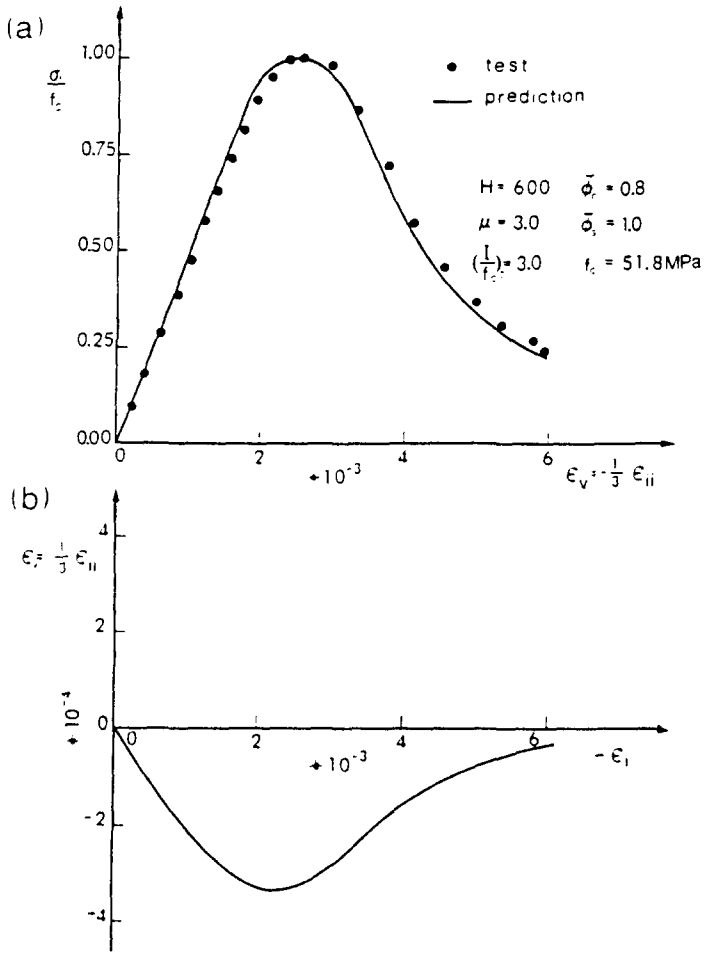

Fig. 12. Simulation of unstable response under uniaxial compression[26].

the most important trends of concrete behaviour under static loading, e.g. compaction–dilatancy transition, sensitivity of material characteristics to confining pressure, the phenomenon of a continuous ductile–brittle transition. In addition to elastic properties, only one material constant f_c is required (or two constants f_c and f_t if the latter is available) to completely define the material response in a hardening regime. A very attractive feature of the model is the fact that both brittle and ductile behaviour are described within the same phenomenological framework. This is certainly advantageous in the context of future numerical implementations.

The effectiveness of the model has been verified for a number of stress paths. The numerical predictions are, in general, quite satisfactory. The model does not predict plastic deformations for a hydrostatic path which is assumed to be a neutral one. Recognizing this limitation, it is believed however, that such a path is unlikely to arise in the context of a boundary value problem.

The applicability of the model is, at the present time, restricted to monotonic loading histories as no irreversible deformations are accounted for during stress reversals. Extension of this concept to cover the cases of fluctuating load is currently under investigation.

REFERENCES

1. L. Cedolin, Y. R. J. Crutzen and S. D. Poli, Triaxial stress–strain relationships for concrete. *J. Engng Mech. Div. ASCE* **103**(EM3), 423–439 (1977).
2. T. C. Y. Liu, A. H. Nilson and F. O. Slate, Biaxial stress–strain relations for concrete. *J. Struct. Div. ASCE* **98**(ST5), 1025–1034 (1972).

3. R. Palaniswamy and S. P. Shah, Fracture and stress–strain relationship of concrete under triaxial compression. *J. Struct. Div. ASCE* **100**(ST5), 901–916 (1974).
4. A. C. T. Chen and W. F. Chen, Constitutive relations for concrete. *J. Engng Mech. Div. ASCE* **101**(EM4), 465–481 (1975).
5. K. J. William and E. P. Warnke, Constitutive model for the triaxial behaviour of concrete. *Proceedings of IABSE Seminar on Concrete Structures Subjected to Triaxial Stress*, Bergamo, Italy, pp. 1–31 (1975).
6. D. J. Han and W. F. Chen, A nonuniform hardening plasticity model for concrete materials. *Mech. Mater.* **4**, 283–302 (1985).
7. Z. P. Bazant and P. D. Bhat, Endochronic theory of inelasticity and failure of concrete. *J. Engng Mech. Div. ASCE* **102**(EM4), 701–722 (1976).
8. Z. P. Bazant and C. L. Shieh, Endochronic model for nonlinear triaxial behaviour of concrete. *Nucl. Engng Des.* **47**, 305–315 (1978).
9. Z. P. Bazant and S. S. Kim, Plastic-fracturing theory for concrete. *J. Engng Mech. Div. ASCE* **105**(EM3), 407–428 (1979).
10. A. Dragon and Z. Mroz, A continuum model for plastic–brittle behaviour of rock and concrete. *Int. J. Engng Sci.* **17**, 121–137 (1979).
11. W. F. Chen, *Plasticity in Reinforced Concrete*. McGraw-Hill, New York (1982).
12. J. Jiang and S. Pietruszczak, Convexity of yield loci for pressure sensitive materials. *Comput. Geotechnics* (to be published).
13. F. B. Lin and Z. P. Bazant, Convexity of smooth yield surface of frictional material. *J. Engng Mech. ASCE* **112**(11), 1259–1262 (1986).
14. H. B. Poorooshasb and S. Pietruszczak, On yielding and flow of sand; a generalized two-surface model. *Comput. Geotechnics* **1**(1), 33–58 (1985).
15. J. W. Rudnicki and J. R. Rice, Conditions for the localization of deformation in pressure-sensitive dilatant materials. *J. Mech. Phys. Solids* **23**, 371–394 (1975).
16. S. Pietruszczak and Z. Mroz, Finite element analysis of deformation of strain softening materials. *Int. J. Numer. Meth. Engng* **17**, 327–334 (1981).
17. M. D. Kotsovos and J. B. Newman, A mathematical description of the deformation behaviour of concrete under complex loading. *Mag. Concr. Res.* **31**(107), 77–90 (1979).
18. H. Kupfer, H. K. Hilsdorf and H. Rusch, Behaviour of concrete under biaxial stress. *Proc. Am. Concr. Inst.* **66**(8), 656–666 (1969).
19. M. D. Kotsovos, Mathematical description of the strength properties of concrete under generalized stress. *Mag. Concr. Res.* **31**(108), 151–158 (1979).
20. N. J. Gardner, Triaxial behaviour of concrete. *Proc. Am. Concr. Inst.* **66**(2), 136–146 (1969).
21. L. L. Mills and R. M. Zimmerman, Compressive strength of plain concrete under multi-axial loading conditions. *Proc. Am. Concr. Inst.* **69**(10), 802–807 (1970).
22. P. Launay and H. Gachon, Strain and ultimate strength of concrete under triaxial stress. *Special Publ. Am. Concr. Inst.* **SP-34**, 269–282 (1970).
23. J. Chinn and R. M. Zimmerman, Behaviour of plain concrete under various high triaxial compression loading conditions. Technical Report No. WL TR 64-163, Air Force Weapons Laboratory, Albuquerque, New Mexico.
24. V. S. Gopalaratnam and S. P. Shah, Softening response of plain concrete in direct tension. *J. Am. Concr. Inst.* **82**(3), 310–323 (1985).
25. W. H. Dilger, R. Koch and R. Kowalczyk, Ductility of plain and confined concrete under different strain. *J. Am. Concr. Inst.* **81**(1), 73–81 (1984).
26. P. T. Wang, S. P. Shah and A. E. Naaman, Stress–strain curves of normal and lightweight concrete in compression. *J. Am. Concr. Inst.* **75**(11), 603–611 (1978).
27. J. G. M. van Mier, Strain-softening of concrete under multiaxial loading conditions. Ph.D. Thesis, Eindhoven University of Technology, Eindhoven, The Netherlands (1984).

APPENDIX A. DETERMINATION OF CONSTITUTIVE TENSOR

According to eqn (24), the material response is governed by an incremental constitutive relation

$$d\sigma_{ij} = D^{ep}_{ijkl}\, d\varepsilon_{kl}$$

in which D^{ep}_{ijkl} is a fourth-order tensor defined by

$$D^{ep}_{ijkl} = D^{e}_{ijkl} - \frac{D^{e}_{ijpq}\dfrac{\partial \Psi}{\partial \sigma_{pq}}\dfrac{\partial f}{\partial \sigma_{mn}} D^{e}_{mnkl}}{H_e + H_p}$$

where

$$H_e = \frac{\partial f}{\partial \sigma_{pq}} D^{e}_{pqrs} \frac{\partial \Psi}{\partial \sigma_{rs}}; \quad H_p = -\frac{\partial f}{\partial \beta}\frac{\partial \beta}{\partial \xi}\left(\mathrm{dev}\,\frac{\partial \Psi}{\partial \sigma_{ij}}\,\mathrm{dev}\,\frac{\partial \Psi}{\partial \sigma_{ij}}\right)^{1/2} \Phi.$$

To specify the form of D^{ep}_{ijkl} the expressions defining the appropriate gradient tensors have to be provided. The gradient of $f = 0$ can be written in the form

$$\frac{\partial f}{\partial \sigma_{ij}} = \frac{\partial f}{\partial I}\frac{\partial I}{\partial \sigma_{ij}} + \frac{\partial f}{\partial \bar{\sigma}}\frac{\partial \bar{\sigma}}{\partial \sigma_{ij}} + \frac{\partial f}{\partial \theta}\frac{\partial \theta}{\partial \sigma_{ij}}.$$

From eqns (1), defining the stress invariants, one obtains

$$\frac{\partial I}{\partial \sigma_{ij}} = -\delta_{ij}; \quad \frac{\partial \bar{\sigma}}{\partial \sigma_{ij}} = \frac{s_{ij}}{2\bar{\sigma}}; \quad \frac{\partial J_3}{\partial \sigma_{ij}} = s_{ik}s_{kj} - \tfrac{2}{3}\bar{\sigma}^2\delta_{ij}$$

so that

$$\frac{\partial \theta}{\partial \sigma_{ij}} = \frac{\partial \theta}{\partial \bar{\sigma}}\frac{\partial \bar{\sigma}}{\partial \sigma_{ij}} + \frac{\partial \theta}{\partial J_3}\frac{\partial J_3}{\partial \sigma_{ij}}$$

where

$$\frac{\partial \theta}{\partial \bar{\sigma}} = \frac{3\sqrt{(3)}J_3}{2\bar{\sigma}^4\cos 3\theta}; \quad \frac{\partial \theta}{\partial J_3} = -\frac{\sqrt{3}}{2\bar{\sigma}^3\cos 3\theta}.$$

Equations (6), (3) and (4), which define the yield locus, lead to

$$\frac{\partial f}{\partial I} = -\beta(\xi)g(\theta)\left\{\frac{K_1(1-K)}{Kf_c}\left(1 - \frac{g(\theta)(\sqrt{(1+a)} - \sqrt{(1-a\sin 3\theta)})}{\sqrt{(1+a)} - \sqrt{(1-a)}}\right) + \frac{1}{[2a_2(\bar{\sigma}_c/f_c) + a_1]}\right\}$$

$$\frac{\partial f}{\partial \bar{\sigma}} = 1.0$$

$$\frac{\partial f}{\partial \theta} = -\frac{3a(1-K)g(\theta)\bar{\sigma}\cos 3\theta}{2K(\sqrt{(1+a)} - \sqrt{(1-a)})\sqrt{(1-a\sin 3\theta)}}.$$

In order to define the current plastic potential surface, the following numerical procedure can be implemented.

(1) *For* $\Psi_0 \geq 0$ (*or* $\eta_c \leq \eta_0$)

Referring to Fig. 2, define the parameter η_c as

$$\eta_c = \frac{\bar{\sigma}^*}{g(\theta)(a_1 f_c + I^*)}$$

where, according to eqns (5) and (11)

$$\bar{\sigma}^* = \tfrac{1}{2}\alpha g(\theta)\frac{f_c}{a_2}\left[-a_1 + \sqrt{\left(a_1^2 + 4a_2\left(a_1 + \frac{I^*}{f_c}\right)\right)}\right].$$

Substituting the above relations into eqn (10) and noting that $\bar{I}_0 = e(a_1 f_c + I^*)$, an algebraic equation in terms of I^* is obtained. After solving this equation, an appropriate value of η_c can be determined which uniquely defines the current plastic potential

(2) *For* $\Psi_0 \leq 0$

The value of parameter η_0, eqn (12), can be directly substituted in eqn (10). Noting that $\bar{I}_0 = ea_0 f_c$, eqn (10) can be solved for a_0, which completely defines $\Psi = 0$.

Once the current plastic potential surface has been identified, the gradient tensor can be evaluated from

$$\frac{\partial \Psi}{\partial \sigma_{ij}} = \frac{\partial \Psi}{\partial I}\frac{\partial I}{\partial \sigma_{ij}} + \frac{\partial \Psi}{\partial \bar{\sigma}}\frac{\partial \bar{\sigma}}{\partial \sigma_{ij}} + \frac{\partial \Psi}{\partial \theta}\frac{\partial \theta}{\partial \sigma_{ij}}$$

in which

$$\frac{\partial \Psi}{\partial I} = -\frac{\bar{\sigma}}{I} + \eta_c g(\theta)$$

$$\frac{\partial \Psi}{\partial \bar{\sigma}} = 1.0$$

$$\frac{\partial \Psi}{\partial \theta} = -\frac{3a(1-K)g(\theta)\bar{\sigma}\cos 3\theta}{2K(\sqrt{(1+a)} - \sqrt{(1-a)})\sqrt{(1-a\sin 3\theta)}}.$$

Finally, in view of eqns (6) and (7)

$$\frac{\partial f}{\partial \beta} = -g(\theta)\bar{\sigma}_c; \quad \frac{\partial \beta}{\partial \xi} = \frac{A}{(A + B\xi)^2} \quad \text{(strain hardening regime only)}$$

which completely defines the plastic hardening modulus H_p.

APPENDIX B. SPECIFICATION OF FUNCTION $\bar{\phi}_s$ AND CONSIDERATIONS ON STATIC ADMISSIBILITY

In Section 2, the strain softening phenomenon has been described by employing the concept of an equivalent continuum, the response of which is sensitive to the actual physical dimensions. The "size effect" has been incorporated through the constant $\bar{\phi}_s$, eqn (13b), which is supposed to relate the rate of strain softening to the geometrical aspects. Instead of considering the details of the sample geometry, assume, for simplicity, that its total volume constitutes a characteristic parameter which affects the softening response, i.e.

$$\bar{\phi}_s = \phi_s(I, V) = \text{const.}$$

in which V represents the volume of the sample.

The function $\bar{\phi}_s$ can be assumed in the following general form

$$\bar{\phi}_s = 1 + \alpha_1(I)\alpha_2\left(\frac{V}{V_s}\right)$$

where V_s denotes a representative (or standard) volume for which the strain softening characteristics are assumed to be known. The function α_2 should be selected in such a manner as to reflect a progressive increase in the rate of strain softening with increasing V/V_s ratio. Moreover, for $V = V_s$ there must be $\alpha_2 = 0$ which implies $\bar{\phi}_s = 1$. Assume, for example, the following simple representation

$$\alpha_2\left(\frac{V}{V_s}\right) = \left(\frac{V}{V_s}\right)^{\lambda} - 1.$$

In the above equation λ represents a constant.

The degree of sensitivity to geometrical aspects may vary with the confining pressure. This is accounted for by introducing the function $\alpha_1(I)$. In general, this function will assume the value from the interval $0 \leqslant \alpha_1 \leqslant 1$. $\alpha_1 = 0$ implies that the strain softening characteristics remain unaffected by the volume of the sample, whereas $\alpha_1 = 1$ expresses maximum sensitivity. As an example, the following trigonometric function may be considered:

$$\alpha_1(I) = \sin\left[\frac{a_1 + (I/f_c)_1}{a_3(I/f_c)_T}\right]\pi.$$

Here, $I \to -a_1 f_c$ and $I \to I_T$ yields $\alpha_1 \to 0$, whereas $\max \alpha_1 = 1$. Figure B1 shows the strain softening characteristics for different V/V_s ratios as predicted by the above specified functions.

Incorporation of $\bar{\phi}_s$ in eqn (13b), requires further investigation concerning the static admissibility of the $\bar{\sigma} - \bar{\varepsilon}$ characteristics. During the strain softening phase a progressive decrease in $\bar{\sigma}$ must be accompanied by the corresponding increase in the value of $\bar{\varepsilon}$, otherwise an abrupt loss of equilibrium will take place. In mathematical terms, the following conditions must be satisfied:

$$d\bar{\varepsilon}^e + d\bar{\varepsilon}^p > 0$$

where the superscripts refer to the elastic and plastic part of $d\bar{\varepsilon}$, respectively.

According to eqns (8)

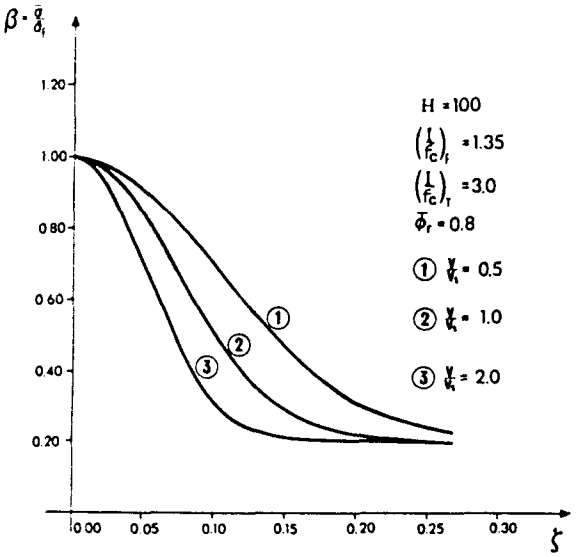

Fig. B1. Influence of $\bar{\phi}_s$ on the rate of strain softening ($\alpha_1 = 1$).

$$\frac{d\beta}{d\xi} = \Phi \frac{d\beta}{d\bar{\varepsilon}^p}$$

so that

$$d\bar{\varepsilon}^p = \frac{\Phi}{\beta'(\xi)} d\beta.$$

For the elastic part

$$d\bar{\varepsilon}^e = \frac{1}{\sqrt{(2)G}} d\bar{\sigma} = \frac{\bar{\sigma}_f}{\sqrt{(2)G}} d\beta$$

where G represents the elastic shear modulus.

Combining the expressions for $d\bar{\varepsilon}^p$ and $d\bar{\varepsilon}^e$, one obtains

$$\left(\frac{\bar{\sigma}_f}{\sqrt{(2)G}} + \frac{\Phi}{\beta'(\xi)} \right) d\beta > 0.$$

In view of $d\beta < 0$, the above inequality reduces to

$$\frac{\bar{\sigma}_f}{\sqrt{(2)G}} + \frac{\Phi}{\beta'(\xi)} < 0$$

or, after a simple rearrangement

$$\frac{d\beta}{d\xi} > -\sqrt{(2)G} \frac{\Phi}{\bar{\sigma}_f}.$$

For an arbitrary I, the function $d\beta/d\xi$ reaches its minimum when

$$\frac{d^2\beta}{d\xi^2} = 0.$$

In order to find this minimum let us simplify the function $\beta(\xi)$ in eqn (13a) to

$$\beta(\xi) \approx \beta_f \{1 - \phi_f [1 - e^{-C(\xi - \xi_f)^2}]\}.$$

After differentiation with respect to ξ, one obtains

$$\frac{d^2\beta}{d\xi^2} = -2\phi_f C \beta_f e^{-C(\xi - \xi_f)^2} [1 - 2C(\xi - \xi_f)^2] = 0$$

which leads to

$$\xi = \xi_f + \sqrt{\left(\frac{1}{2C} \right)}$$

so that

$$\min \left(\frac{d\beta}{d\xi} \right) = -\phi_f \beta_f \sqrt{(2C)}\, e^{-1/2}.$$

Substituting the above equation in the criterion for static admissibility, one obtains

$$C < \frac{[G(\Phi/\bar{\sigma}_f)]^2 e^4}{(\bar{\sigma}_f \beta_f)^2}.$$

Finally, in view of eqn (13b), the following inequality is arrived at:

$$H < \frac{G^2 e^4}{\phi_f^2 \beta_f \phi_s \left[\dfrac{(I/f_c)_f - (I/f_c)_f}{a_3 + (I/f_c)_f} \right]} \left(\frac{\Phi}{\bar{\sigma}_f} \right)^2$$

which represents a constraint imposed on the selection of H in eqn (13b).